

## Numerical investigation of influence of cross-sectional dimensions of flow channels on PEM fuel cell performance

Mahmut Kaplan

Amasya University, Technology Faculty, Department of Mechanical Engineering, Amasya, Turkey, mahmut.kaplan@amasya.edu.tr

Submitted: 30.01.2021

Accepted: 24.05.2021

Published: 30.06.2021



**Abstract:** Proton exchange membrane fuel cell (PEMFC) has acquired increasing importance because of operating at higher efficiency and producing environmentally friendly power at low temperatures over the past decade. Flow channel as a vital part of PEMFC plays a critical role for augmenting the performance of PEMFC. In this paper, a single phase, 3-D model is generated to examine impact of the channel cross-section geometry on the cell performance. 15 different simulation cases were gained by altering the flow channel width and depth from 0.2 to 1.6 mm for the fixed depth and width of 1 mm, respectively. In the base case, the channel dimensions are 1.0 mm width and depth. The results revealed that decreasing depth and width of the channel enhanced the current density thanks to increasing gas velocity in the flow channels of the anode and cathode at the expense of increased pressure drop. The cases having the channel cross-sectional dimensions of 0.2 x 0.1 mm and 0.1 x 0.2 mm (channel width x depth) enhanced the current density about 57% and 45% at 0.4 V compared to the base case. Besides, oxygen consumption and water production in the cathode side are also remarkably increased in these cases. However, the channel cross-sectional size of 0.8 x 1 mm case which increases the current density 2.5% at 0.4 V in comparison with the base case can be best option by taking into consideration pressure drop into the flow channels.

**Keywords:** CFD, Flow channel dimensions, Optimization, PEMFC, Pressure drop

Cite this paper as: Kaplan, M. Numerical investigation of influence of cross-sectional dimensions of flow channels on PEM fuel cell performance. *Journal of Energy Systems* 2021, 5(2), 137-148, DOI: 10.30521/jes.871018

© 2021 Published by peer-reviewed open access scientific journal, JES at DergiPark (<https://dergipark.org.tr/en/pub/jes>)

Nomenclature		Greek letter	
$C$	Molar concentration ( $\text{mol m}^{-3}$ )	$\alpha$	Transfer coefficient (dimensionless)
$D$	Diffusion coefficient ( $\text{m}^2 \text{s}^{-1}$ )	$\gamma$	Concentration exponent
$F$	Faraday constant ( $\text{C kmol}^{-1}$ )	$\varepsilon$	Porosity
$h_L$	Enthalpy change for condensation or vaporization of water ( $\text{J kg}^{-1}$ )	$\zeta$	Specific active surface area ( $\text{l m}^{-1}$ )
$h_{\text{reaction}}$	Enthalpy change of electrochemical reactions ( $\text{J kg}^{-1}$ )	$\eta$	Overpotential (V)
$I$	Current density ( $\text{A m}^{-2}$ )	$\mu$	Viscosity ( $\text{kg m}^{-1} \text{s}^{-1}$ )
$j$	Exchange current density ( $\text{A m}^{-2}$ )	$\rho$	Density ( $\text{kg m}^{-3}$ )
$K$	Permeability ( $\text{m}^2$ )	$\sigma$	Electrical conductivity ( $\text{l } \Omega^{-1} \text{ m}^{-1}$ )
$k$	Thermal conductivity ( $\text{W m}^{-1} \text{K}^{-1}$ )	$\phi$	Electric potential (V)
$M_w$	Molecular weight ( $\text{kg mol}^{-1}$ )	<b>Subscript</b>	
$P$	Pressure (Pa)	<i>an</i>	Anode
$R$	Universal gas constant ( $\text{J mol}^{-1} \text{K}^{-1}$ )	<i>cat</i>	Cathode
$R_{\text{ohm}}$	Ohmic resistivity ( $\Omega \text{m}^2$ )	<i>eff</i>	Effective
$S_h$	Energy source term	<i>k</i>	Chemical species
$S_k$	Species source term	<i>mem</i>	Membrane
$S_m$	Momentum source term	<i>ref</i>	Reference
$T$	Temperature (K)	<i>sol</i>	Solid
$\vec{u}$	Velocity vector ( $\text{m s}^{-1}$ )		
$V_{oc}$	Open-circuit voltage (V)		

## 1. INTRODUCTION

In today's world, alternative energy sources are sought to replace the traditional energy sources owing to environmental aspects and energy sources limit. Hydrogen is a promising fuel source to supply the world's energy demand. PEM fuel cell changes the chemical energy into electricity by oxidizing hydrogen as a fuel. PEMFC has attracted increasing attention owing to operating at low temperatures and suitability for using various applications such as transportation, stationary, backup, and portable power [1]. A typical PEMFC unit comprises of a membrane, gas diffusion layers (GDLs), catalyst layers (CLs), and bipolar plates in which flow channels are machined. The following electrochemical reactions occur in the CLs:



In PEMFC, flow channels provide distribution of reactants (hydrogen and oxygen) and remove water and heat [2]. Besides, properly designed flow channels is a key factor to achieve uniform flow distribution, giving rise to an enhancement in the cell efficiency [3]. Recent numerical studies demonstrated that PEMFC performance can be improved by altering PEMFC flow channel geometries and dimensions [4-16]. Liu et al. [7] formed a computational model to optimize flow channel cross-sectional area and current collector rib dimensions. They concluded that reducing both the flow channel total width and the rib-to-total width ratio resulted in enhancing the power output of PEMFC.

Khazaei et al. [9] evaluated the impact of increasing number of channels and modifying channel cross-section shapes such triangular, rectangular, and elliptical on the performance using a three-dimensional single-phase model. They concluded that the cell performance enhanced by increasing number of channels for all channel cross-section geometries and the best performance was gained with reducing the cross-section area of rectangular channel 2 to 1 mm<sup>2</sup>. Cooper et al. [10] examined relationship between the channel length to width ratio and performance improvement in PEMFC having interdigitated channels. Their results demonstrated that decreasing the aspect ratio by reducing the channel length led to higher overall performance. Chowdhury et al. [11] improved a 3-D isothermal single-phase model to optimize the width ratio of the channel/land for PEMFC. They reported that both channel and land width were equally important to augment the cell current density and the case with 1 mm channel and land widths might be best appropriate dimensions considering current density and pressure drop inside the flow channel.

Kerkoub et al. [12] established a computational model to examine different flow channel geometry containing interdigitated, serpentine, and parallel having different channel to rib width ratios. They discovered that the channel geometry and channel/rib width ratio considerably affected PEMFC performance at low operating voltage whereas they had a little impact on the cell efficiency at high operating voltage. Carcada et al. [14] scrutinized the influence of the serpentine channel patterns (7, 11, and 14 channels) and the channel cross-sectional dimensions on performance of PEMFC with a large size of active area. The results indicated that the cell performed better when increasing number of serpentine channels and decreasing channel and land width, particularly at higher current densities. Mohammadi et al. [15] explored the influence of various channel cross-section forms on the power density and pressure drop using ANSYS Fluent CFD software. They notified that the cross-section form with trapezoidal top half and inverted trapezoidal bottom half considerably enhanced power density, but this cross-section form increased pressure drop compared to rectangular cross-section form.

The goal of this study is to introduce a single-phase CFD model to evaluate the impact of the channel cross-sectional geometry (the channel width and depth) on the PEMFC performance. This study is structured as follows. In Section 2, the detailed description of PEMFC model including some assumptions is introduced. Section 3 illustrates the simulation results and their discussion. Lastly, the main conclusions obtained from the present numerical work are given in Section 4.

## 2. MODEL DESCRIPTION

The geometric model used in this study was constructed using SOLIDWORKS software. Then the geometry is meshed ANSYS Workbench platform. To specify the physical domains included in the FLUENT Fuel Cell module, numerical grid is separated into 9 zones containing anode and cathode current collector, flow channel, GDL, CL and a membrane in Figure 1.

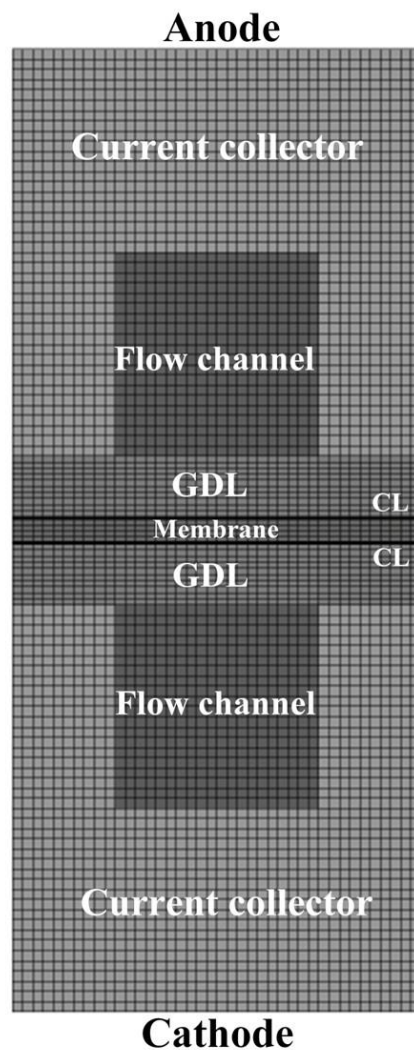


Figure 1. Computational grid of PEMFC model

The cell length and width are 70 and 2 mm, respectively. The thickness of the membrane, GDLs and CLs are 0.108, 0.3 and 0.0129 mm, respectively. The channel length and the membrane, GDL and CL thickness are the same for all cases. For the base case, the channel width and depth are 1 mm. The values of geometrical parameters used in the base case are same with the experimental study carried out by Wang et al. [17]. The design properties and operating conditions employed for the base and other cases are demonstrated in Table 1.

Table 1. Operating conditions and electrochemical characteristics of PEMFC

Parameter	Value
Anode mass fraction of H <sub>2</sub> at the inlet	0.2
Anode mass fraction of H <sub>2</sub> O at the inlet	0.8
Cathode mass fraction of O <sub>2</sub> at the inlet	0.2
Cathode mass fraction of H <sub>2</sub> O at the inlet	0.1
Reference H <sub>2</sub> and H <sub>2</sub> O diffusion	$7.33 \times 10^{-5} \text{ m}^2/\text{s}$ [18]
Reference O <sub>2</sub> diffusion	$2.13 \times 10^{-5} \text{ m}^2/\text{s}$ [18]
Reference species diffusion	$4.9 \times 10^{-5}$ [18]
Operating temperature	343 K [17]
Operating pressure	101.325 kPa [17]
GDLs and CLs porosity	0.5 [19]
GDLs and CLs viscous resistance	$1 \times 10^{12} \text{ 1/m}^2$ [19]
CL surface/volume ratio	200000 1/m
Reference exchange current density (anode)	4000 A/m <sup>2</sup>
Reference exchange current density (cathode)	0.1 A/m <sup>2</sup>
Open-circuit voltage	0.94 V

The operational data related to inlet mass fractions of anode and cathode gases in Table 1 is obtained based on the work by Biyikoglu et al. [18].

### 2.1. Geometrical interest

In this study, different cases are obtained by changing flow channel width and depth in the range 0.2-1.6 mm with intervals of 0.2 mm for the fixed depth and width of 1 mm, respectively as illustrated in Figure 2.

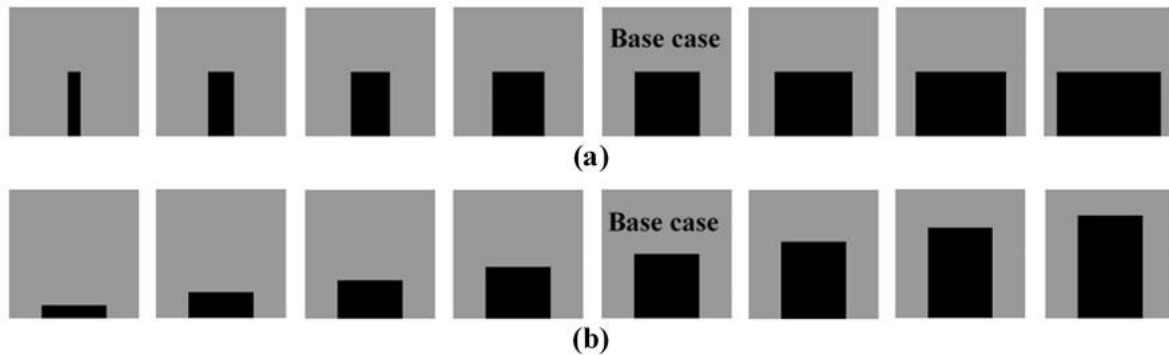


Figure 2. Flow channel cases a) various channel width with the fixed depth cases b) various channel depths with fixed width cases

### 2.2. Assumptions

The numerical model has been improved on the grounds of the following assumptions:

- (a) The steady state condition is considered.
- (b) The flow is single phase, incompressible and laminar.
- (c) The gas mixtures behave as perfect gases.
- (d) The GDL, CL and membrane are considered as isotropic and homogenous porous medium.
- (e) Only gas mixtures are present in flow channels.

### 2.3. Governing transport equations

Mass, momentum, energy, species, and current equations are used to simulate physical phenomena taking place in the PEMFC. Conservation of mass is identified by:

$$\nabla(\rho\vec{u}) = 0 \quad (3)$$

Conservation of momentum is described by:

$$\frac{1}{(\varepsilon^{eff})^2} \nabla(\rho\vec{u}\vec{u}) = -\nabla P + \nabla(\mu\nabla\vec{u}) + S_m \quad (4)$$

where  $\varepsilon^{eff}$  is effective porosity of porous mediums.  $S_m$  is the source term based on Darcy's law for porous flow fields [20].

$$S_m = -\frac{\mu}{K} \vec{u} \quad (5)$$

where  $K$  is the permeability inside porous medium. Conservation equations for species can be written as:

$$\nabla(\vec{u}C_k) = \nabla(D_k^{eff} \nabla C_k) + S_k \quad (6)$$

where  $D_k^{eff}$  is the effective diffusion coefficient for  $k$  species which can be calculated via Bruggeman model including the impacts of the porosity ( $\varepsilon$ ) and tortuosity in GDLs and CLs [21].

$$D_k^{eff} = D_k \varepsilon^{1.5} \quad (7)$$

The source term in the species equations,  $S_k$  is defined for hydrogen, oxygen, and water, as follows:

$$S_{H_2} = -\frac{M_{w,H_2}}{2F} R_{an} \quad (8)$$

$$S_{O_2} = -\frac{M_{w,O_2}}{4F} R_{cat} \quad (9)$$

$$S_{H_2O} = \frac{M_{w,H_2O}}{2F} R_{cat} \quad (10)$$

where  $R_{an}$  and  $R_{cat}$  are volumetric transfer current of anode and cathode in  $A\ m^{-3}$ , respectively. Conservation of energy can be represented by:

$$\nabla(\rho\vec{u}T) = \nabla(k^{eff} \nabla T) + S_h \quad (11)$$

The source term in the energy conservation equation,  $S_h$ , is given by:

$$S_h = h_{reaction} + h_L - R_{an,cat} \eta_{an,cat} + I^2 R_{ohm} \quad (12)$$

where  $h_{reaction}$  and  $h_L$  are the change of enthalpy as owing to the electrochemical reactions and condensation or vaporization of water, respectively.  $\eta_{an,cat}$  is the local surface over potential for the anode and cathode. The following two charge conservation equations are described for representing protonic and electron transport in the membrane and solid conductive material, respectively.

$$\nabla(\sigma_{mem} \nabla \phi_{mem}) + R_{mem} = 0 \quad (13)$$

$$\nabla(\sigma_{sol} \nabla \phi_{sol}) + R_{sol} = 0 \quad (14)$$

where  $\sigma$  is electrical conductivity and  $\phi$  are electrical potential. Subscript *mem* and *sol* denote membrane and solid phase, respectively.  $R_{mem} = +R_{an}$  (anode) and  $R_{mem} = -R_{cat}$  (cathode) for membrane phase. On the other hand,  $R_{sol} = -R_{an}$  (anode) and  $R_{mem} = +R_{cat}$  (cathode) for solid phase.  $R_{an}$  and  $R_{cat}$  are computed based on the Butler–Volmer expression [22]:

$$R_{an} = (\zeta_{an} j_{an}^{ref}) \left( \frac{[H_2]}{[H_2]_{ref}} \right)^{\gamma_{an}} \left( e^{\alpha_{an} F \eta_{an} / RT} - e^{-\alpha_{cat} F \eta_{an} / RT} \right) \quad (15)$$

$$R_{cat} = (\zeta_{cat} j_{cat}^{ref}) \left( \frac{[O_2]}{[O_2]_{ref}} \right)^{\gamma_{cat}} \left( -e^{+\alpha_{an} F \eta_{cat} / RT} + e^{-\alpha_{cat} F \eta_{cat} / RT} \right) \quad (16)$$

$j^{ref}$  is reference exchange current density per surface area.  $F$  represents Faraday's constant,  $F = 9.65 \times 10^7 \text{ C kmol}^{-1}$ .  $\eta_{an}$ , and  $\eta_{cat}$  which are the driving force for the anodic and cathodic reactions can be calculated using following equations:

$$\eta_{an} = \phi_{sol} - \phi_{mem} \quad (17)$$

$$\eta_{cat} = \phi_{sol} - \phi_{mem} - V_{oc} \quad (18)$$

where  $V_{oc}$  is open-circuit voltage.

## 2.4. Boundary conditions

The constant mass flow rates of  $5.398 \times 10^{-6}$  and  $3.294 \times 10^{-5} \text{ kg/s}$  are specified at the anode and cathode flow channel inlet, respectively [18]. A constant pressure of 101.325 kPa is applied at the channel outlet for the anode and cathode. For all computational domains, the internal boundaries are continuous. Both anode and cathode terminals (current collector top faces) are assigned as wall boundary conditions. The anode terminal was grounded. The cathode terminal is set as the constant potential whose maximum value is equal to the open-circuit voltage. The same boundary conditions are used for the base and other simulation cases.

## 3. RESULTS AND DISCUSSIONS

### 3.1. Model validation

The computational model used in the present work has been confirmed with experimental data gained from the work of Wang et al. [17] in Figure 3.

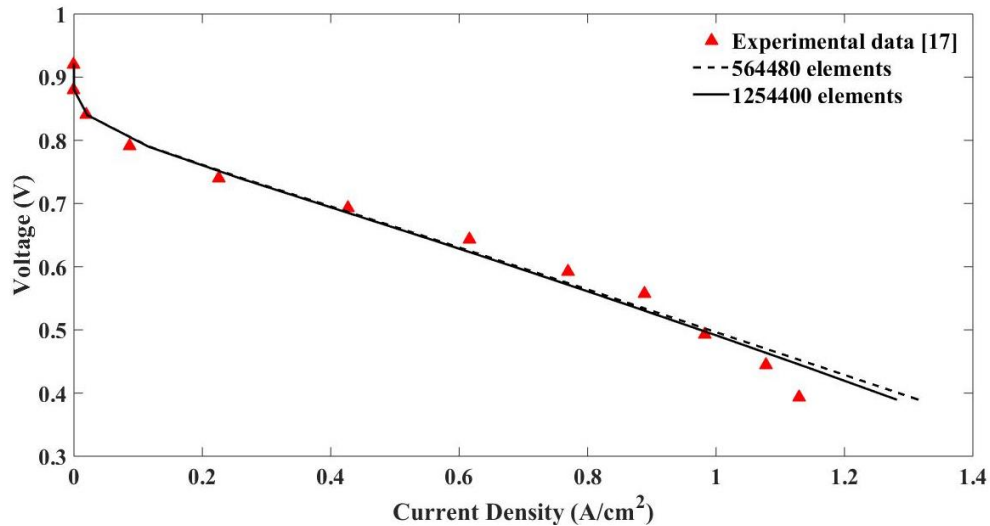


Figure 3. Comparison mathematical model with experimental data [17]

Two different mesh sizes with 564480 and 1254400 hexahedral elements are inspected. It is clearly shown in Figure 3 that for both sizes, the estimated results are in well agreement with the measured data, especially at low and medium current densities. However, the 3D simulation tends to overpredict the measured data at high current densities. The reason may be that the present model disregards the liquid water presence in the CLs and GDLs which leads to the decrease of the GDL and CL porosity and the increase of gas mass transfer resistance. Since the mesh of 1254400 elements leads to more accurate results at lower voltages, this mesh is used. In addition, the same mesh size is obtained by dividing the width and depth of bipolar plate in 40 quadrilateral elements for all cases.

### 3.2. Impact of cross-sectional dimensions of flow channel on current density

Figure 4 shows the estimated current densities for the variation of the channel width between 0.2 and 1.6 mm with the fixed depth of 1 mm at the cell voltage of 0.4, 0.5, and 0.6 V. As can be observed in Figure 4 that the current density increases almost linearly with decreasing channel width for the constant depth of 1 mm until 0.4 mm channel width, but then rapid increase of the current density is observed for 0.2 mm channel width case at 0.4, 0.5 and 0.6 V. Therefore, the highest current densities of 1.97, 1.44 and 0.95 A/cm<sup>2</sup> are obtained with 0.2 mm channel width for V=0.4, 0.5, and 0.6 V, respectively, as indicated in Figure 4. This is expected because reducing channel width leads to enhancement of gas flow velocity and therefore augments the diffusion of the reactant gases to the GDL.

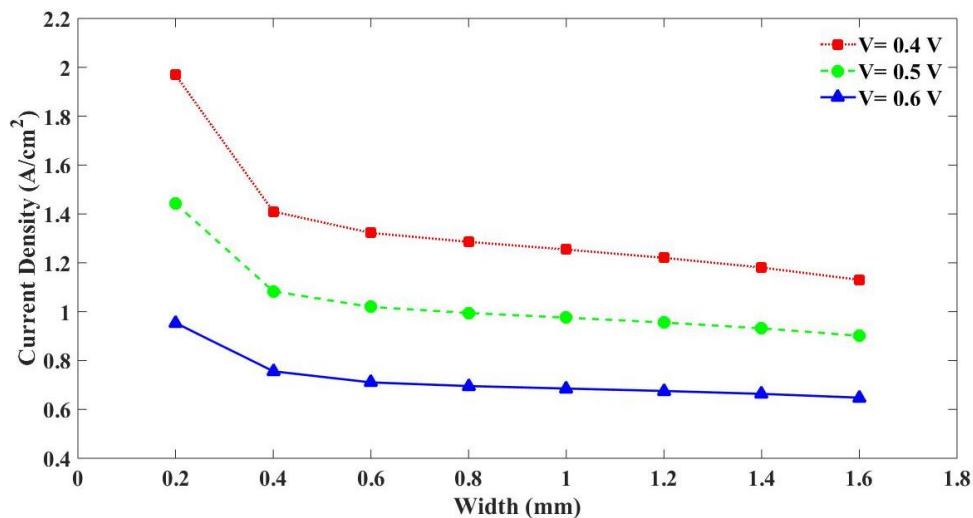


Figure 4. Current density variation for different flow channel width with constant depth of 1 mm at 0.4, 0.5, and 0.6 V

The estimated current densities for the variation of the channel depth in the range of 0.2 to 1.6 mm with the fixed width of 1 mm at the cell voltage of 0.4, 0.5, and 0.6 V are presented in Figure 5.

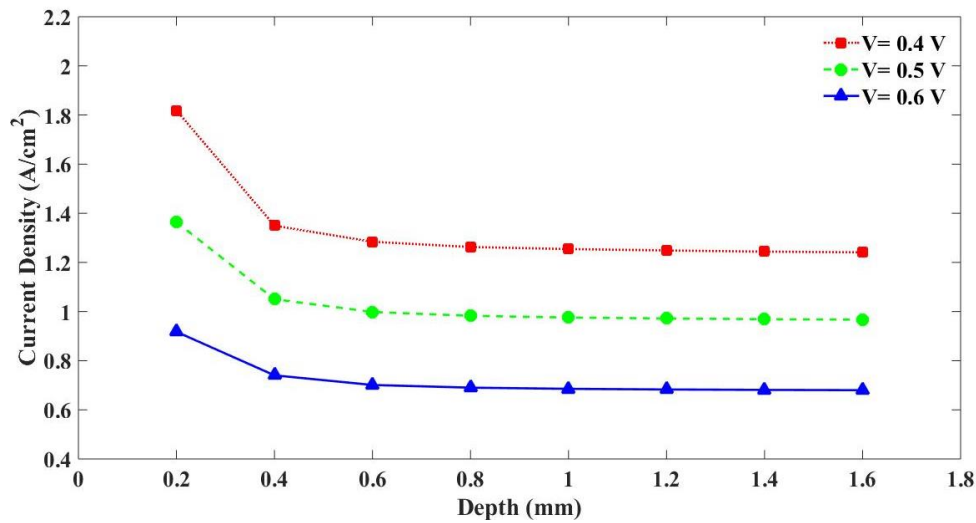


Figure 5. Current density variation for different flow channel depth with constant width of 1 mm at 0.4, 0.5, and 0.6 V

It is demonstrated in Figure 5 that the current density is not significantly changed with decreasing of the channel depth until the channel width of 0.6 mm. Then, the current density is notably increased for 0.4 mm channel depth compared to the base model having 1 mm depth. The highest current densities of 1.82, 1.36 and 0.92 A/cm<sup>2</sup> are obtained with 0.2 mm channel depth for V=0.4, 0.5, and 0.6 V, respectively, as indicated in Figure 5.

Figures 4 and 5 show that decreasing the channel width with the fixed depth is more sensitive to enhance the current density of the PEMFC than decreasing channel depth with the fixed width. This may be on the grounds that the increase of the land area with the decrease of the channel width contributes to minimize ohmic losses by reducing contact resistance between GDL and bipolar plate [23].

### 3.3. Impact of cross-sectional dimensions on oxygen and water distribution

Figures 6 (a), (b) and (c) present the oxygen mass fraction in the cathode flow channel, GDL, and CL at the middle of the cell length for channel cross-sectional dimensions of 0.2 x 1.0, 1.0 x 0.2 and 1.0 x 1.0 mm (channel width x depth) at 0.4 V.

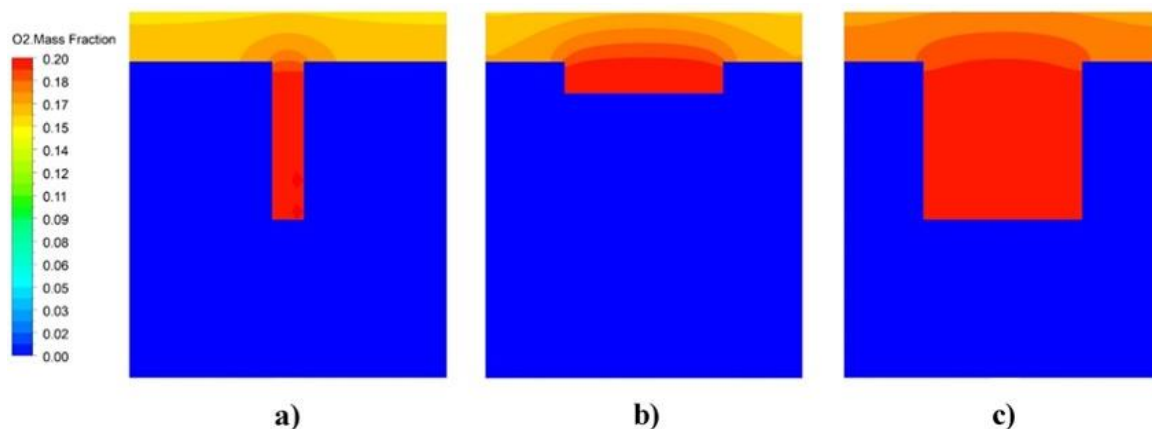


Figure 6. Contour diagrams of O<sub>2</sub> mass fraction in the cathode flow channel, GDL and CL at the middle of the cell length for channel sizes of (a) 0.2 x 1.0 mm (b) 1.0 x 0.2 mm and (c) 1 x 1 mm (base case) at 0.4 V

As can be observed in Figure 6 (a) and (b) that decreasing channel width and depth to 0.2 mm increase consumption of oxygen in CL and GDL compared to the base case in Figure 6 (c) at 0.4 V. These results confirms that 0.2 x 1 mm and 1 x 0.2 mm channel cross-section cases producing higher current densities as shown in Figures 4 and 5 consume more oxygen for the reaction in the cathode catalyst compared to the base case at 0.4 V. Figure 7 (a), (b), and (c) presents the water mass fraction in the cathode flow channel, GDL, and CL at the middle of the cell length for channel cross-sectional sizes of 0.2 x 1.0, 1.0 x 0.2 and 1.0 x 1.0 mm at 0.4 V.

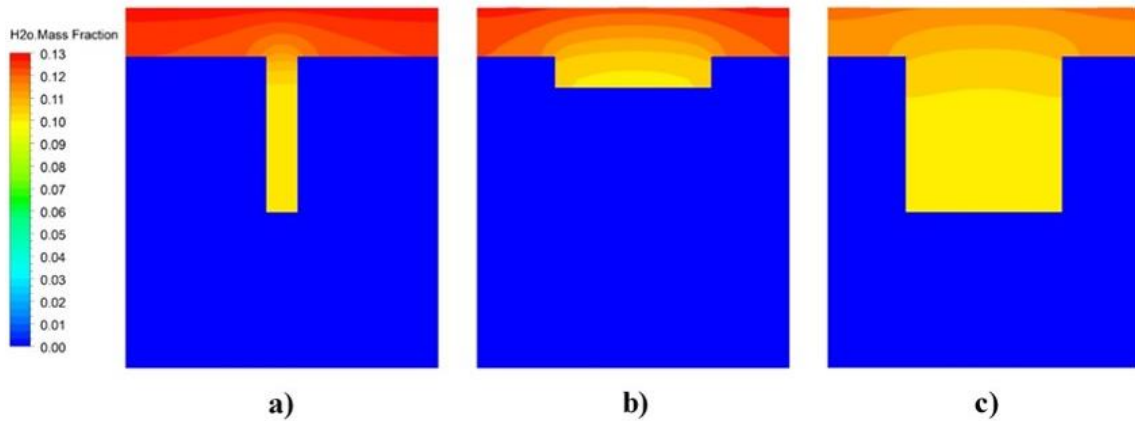


Figure 7. Contour diagrams of water mass fraction in the cathode flow channel, GDL and CL at the middle of the cell length for channel sizes of (a) 0.2 x 1.0 mm (b) 1.0 x 0.2 mm and (c) 1.0 x 1.0 mm (base case) at 0.4 V

Decreasing channel width and depth to 0.2 mm in Figure 7 (a) and (b), respectively increases production of water in CL and GDL compared to base case in Figure 7 (c). It is concluded that reducing the flow channel cross-section dimensions augments O<sub>2</sub> consumption and water production and thus, enhance cell performance.

### 3.4. Impact of cross-sectional dimensions of flow channel on pressure drop

Figure 8 indicates the influence of variation of channel width for fixed depth of 1 mm on pressure drop in the anode and cathode channels for V=0.4, 0.5, and 0.6 V.

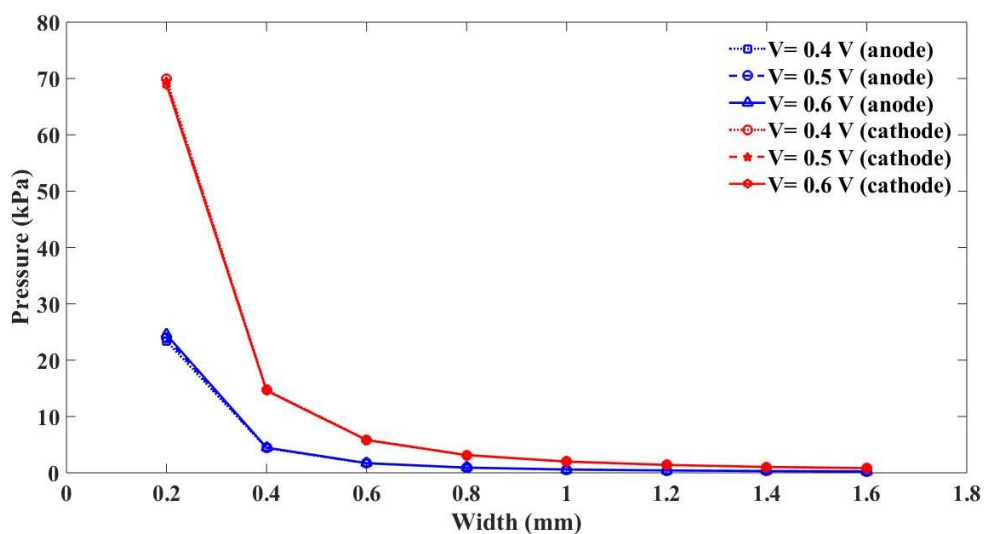


Figure 8. Anode and cathode pressure drop for various flow channel depth with constant width of 1mm for 0.4, 0.5, and 0.6 V

As shown in Figure 8, the decrease of the channel width increases the pressure drop in both channels and the highest pressure drop of 69.88 kPa is observed in the cathode channel with 0.2 mm width and 1.0 mm depth. The effect of variation of channel depth for fixed width of 1 mm on pressure drop in the anode and cathode channels for  $V=0.4, 0.5,$  and  $0.6$  V is shown in Figure 9.

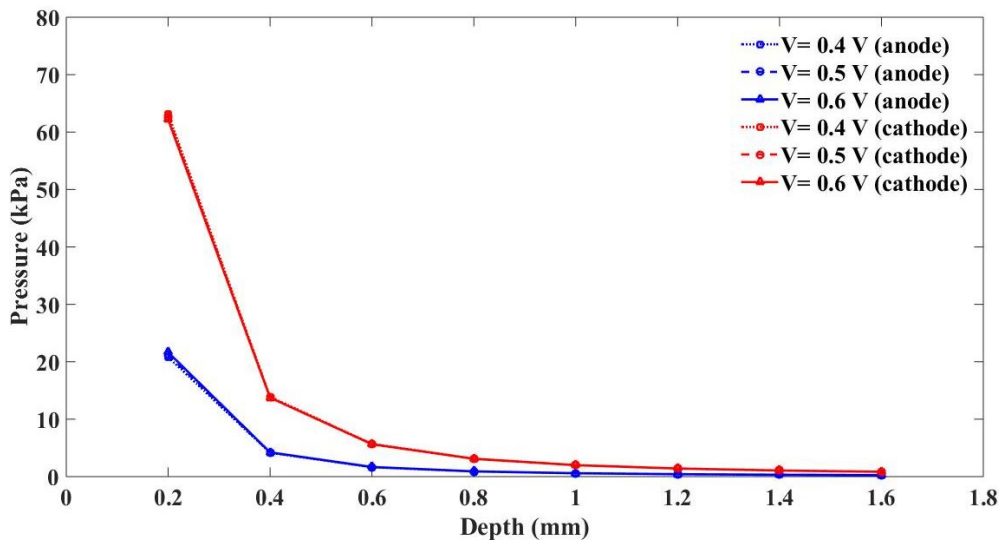


Figure 9. Anode and cathode pressure drop for various flow channel depth with constant width of 1mm for 0.4, 0.5, and 0.6 V

As shown in Figure 9, the decrease of the channel width elevates the pressure drop in both channels and the highest pressure drop of 63.10 kPa is examined in the cathode flow channel having 1.0 mm width and 0.2 mm depth. Figures 8 and 9 indicate that the pressure drop in the cathode channel is much higher than in the anode channel. This may be owing to mixture in the cathode channel being more complicated compared to that of in the anode channel. It is also seen in Figures 8 and 9 that variation of cell voltage is negligible impact on pressure drop inside flow channels.

Excessive pressure drop in the flow channel leads to larger parasitic energy losses and therefore decreases the fuel cell efficiency due to increasing pumping work. Therefore, to choose an appropriate channel cross-section dimensions, the selected cases of current density and pressure drop for 0.4 V are examined in Table 2.

Table 2. Current density and pressure drop for the selected cases at 0.4 V

Cases	width x depth (mm)	Current density (A/m <sup>2</sup> )	Pressure drop (anode/cathode) (kPa)
Different channel width with fixed depth	0.2 x 1.0	1.97	23.39 / 69.88
	0.8 x 1.0	1.29	0.90 / 3.17
	1.6 x 1.0	1.13	0.25 / 0.83
Different channel depth with fixed width	1.0 x 0.2	1.82	20.82 / 63.10
	1.0 x 0.8	1.26	0.90 / 3.12
	1.0 x 1.6	1.24	0.26 / 0.84
Base	1.0 x 1.0	1.25	0.58 / 2.00

As shown in Table 2, the maximum current density is achieved with 0.2 x 1.0 mm channel case. But this case exhibits the largest pressure drop in comparison with other cases. On the other hand, the minimum pressure drop takes place in 1.6 x 1.0 mm channel case. However, this channel case produces minimum current density. Thus, 0.8 x 1.0 mm channel case with 2.5% enhancement in current density compared to base case at 0.4 V can ensure better cell performance concerning current density and pressure drop in the channels.

## 6. CONCLUSIONS

In the present work, a 3-D single phase computational model was improved and verified by the measured data [17] to investigate impact of varying the flow channel dimensions (width and depth) on PEMFC performance. 14 cases compared with the base model and following results are obtained. Below, important findings have been reported:

1. Decreasing channel width have more impact on improving the cell performance than decreasing channel depth because of increasing land area with reducing the channel width results in the decrease of the contact resistance losses.
2. The maximum current density of  $1.97 \text{ A/m}^2$  at 0.4 V is achieved by the channel case with 0.2 mm width and 1.0 depth and for this case, oxygen consumption and water production in cathode CL are higher than that of other cases.
3. The channel gas flow velocity augments with minimising channel cross-section geometry.
4. Reducing either the width or depth of the flow channels results in higher pressure drop in the anode and cathode channels.
5. Voltage variation from 0.4 V to 0.6 V is not significantly affected by pressure drop in the channel. Considering pressure drop, the channel with 0.8 mm width and 1.0 mm depth case with 2.5% enhancement of the current density compared to base model provides better performance.

## REFERENCES

- [1] Barbir F. PEM Fuel Cells: Theory and Practice. London, UK: Elsevier/Academic Press, 2013.
- [2] Wu, HW. A review of recent development: Transport and performance modelling of PEM fuel cells. *Applied Energy* 2016; 165: 81–106, DOI: <https://doi.org/10.1016/j.apenergy.2015.12.075>
- [3] Celik E, Karagoz I. Polymer electrolyte membrane fuel cell flow field designs and approaches for performance enhancement. *Proceedings of the Institution of Mechanical Engineers, Part A: Journal of Power and Energy* 2020; 234(8): 1189–1214, DOI: [10.1177/0957650919893543](https://doi.org/10.1177/0957650919893543)
- [4] Kumar, A, Ramana, GR. Effect of channel dimensions and shape in the flow-field distributor on the performance of polymer electrolyte membrane fuel cells. *Journal Power Sources* 2003; 113: 11–18, DOI: [10.1016/S0378-7753\(02\)00475-5](https://doi.org/10.1016/S0378-7753(02)00475-5)
- [5] Alvarado, BR, Guerrero, AH, Robles, DJ, Li, P. Numerical investigation of the performance of symmetric flow distributors as flow channels for PEM fuel cells. *International Journal of Hydrogen Energy* 2012; 37(1): 436–448, DOI: [10.1016/j.ijhydene.2011.09.080](https://doi.org/10.1016/j.ijhydene.2011.09.080)
- [6] Santamaria, AD, Cooper, NJ, Becton, MK, Park, JW. Effect of channel length on interdigitated flow-field PEMFC performance: A computational and experimental study. *International Journal of Hydrogen Energy* 2013; 38: 16253–16263, DOI: [10.1016/j.ijhydene.2013.09.081](https://doi.org/10.1016/j.ijhydene.2013.09.081)
- [7] Liu, H, Li, P, Wang, K. Optimization of PEM fuel cell flow channel dimensions- Mathematic modeling analysis and experimental verification. *International Journal of Hydrogen Energy* 2013; 38: 9835–9846, DOI: [10.1016/j.ijhydene.2013.05.159](https://doi.org/10.1016/j.ijhydene.2013.05.159)
- [8] Obayopo, SO, Ochende, TB, Meyer, JP. Three-dimensional optimisation of a fuel gas channel of a proton exchange membrane fuel cell for maximum current density. *International Journal of Energy Research* 2013; 37(3): 228–241, DOI: [10.1002/er.1935](https://doi.org/10.1002/er.1935)
- [9] Khazaei, I, Sabadban, H. Numerical study of changing the geometry of the flow field of a PEM fuel cell. *Heat and Mass Transfer* 2016; 52:993–1003, DOI: [10.1007/s00231-015-1621-4](https://doi.org/10.1007/s00231-015-1621-4)
- [10] Cooper, NJ, Santamaria, AD, Becton, MK, Park, JW. Investigation of the performance improvement in decreasing aspect ratio interdigitated flow field PEMFCs. *Energy Conversion and Management* 2017; 136: 307–317, DOI: [10.1016/j.enconman.2017.01.005](https://doi.org/10.1016/j.enconman.2017.01.005)
- [11] Chowdhury, MZ, Genc, O, Toros, S. Numerical optimization of channel to land width ratio for PEM fuel cell. *International Journal of Hydrogen Energy* 2018; 43: 10798–10809, DOI: [10.1016/j.ijhydene.2017.12.149](https://doi.org/10.1016/j.ijhydene.2017.12.149)
- [12] Kerkoub, Y, Benzaoui, A, Haddad, F, Ziari, YK. Channel to rib width ratio influence with various flow field designs on performance of PEM fuel cell. *Energy Conversion and Management* 2018; 174: 260–275, DOI: [10.1016/j.enconman.2018.08.041](https://doi.org/10.1016/j.enconman.2018.08.041)
- [13] Asgharian, H, Afshari, E, Baniasadi, E. Numerical investigation of pressure drop characteristics of gas channels and U and Z type manifolds of a PEM fuel cell stack. *International Journal of Energy Research* 2020; 44(7): 5866–5880, DOI: [10.1002/er.5358](https://doi.org/10.1002/er.5358)

- [14]Carcadea, E, Ismail, MS, Ingham, DB, Patularu, L, Schitea, D, Marinoiu, A, Ebrasu, DI, Mocanu, D, Varlam, M. Effects of geometrical dimensions of flow channels of a large-active-area PEM fuel cell: A CFD study. *International Journal of Hydrogen Energy* 2021; 46(25): 13572-13582, DOI: [10.1016/j.ijhydene.2020.08.150](https://doi.org/10.1016/j.ijhydene.2020.08.150)
- [15]Mohammedi, A, Sahli, Y, Moussa, HB. 3D investigation of the channel cross-section configuration effect on the power delivered by PEMFCs with straight channels. *Fuel* 2020; 263(1): 116713, DOI: [10.1016/j.fuel.2019.116713](https://doi.org/10.1016/j.fuel.2019.116713)
- [16]Zhang, L, Shi, Z. Optimization of serpentine flow field in proton exchange membrane fuel cell under the effects of external factors. *Alexandria Engineering Journal* 2021; 60(1): 421-433, DOI: [10.1016/j.aej.2020.09.007](https://doi.org/10.1016/j.aej.2020.09.007)
- [17]Wang, L, Husar A, Zhou, T, Liu, H. A parametric study of PEM fuel cell performances. *International Journal of Hydrogen Energy* 2003; 28(11): 1263–1272, DOI: [10.1016/S0360-3199\(02\)00284-7](https://doi.org/10.1016/S0360-3199(02)00284-7)
- [18]Biyikoglu, A, Alpat, CO. Parametric study of a single cell proton exchange membrane fuel cell for a bundle of straight gas channels. *Gazi University Journal of Science* 2011; 24(4): 883–899. <https://dergipark.org.tr/tr/pub/gujs/issue/7421/97301>
- [19]Kahveci, EE, Taymaz I. Assessment of single-serpentine PEM fuel cell model developed by computational fluid dynamics. *Fuel* 2018; 117: 51-58, DOI: [10.1016/j.fuel.2017.12.073](https://doi.org/10.1016/j.fuel.2017.12.073)
- [20]Gurau, V, Liu, H, Kakac, S. Two-Dimensional Model for Proton Exchange Membrane Fuel Cells. *AIChE Journal* 1998; 44(11): 2410–2422, DOI: [10.1002/aic.690441109](https://doi.org/10.1002/aic.690441109)
- [21]O’Hayre R, Cha SW, Colella WG, Prinz FB. *Fuel Cell Fundamentals*, New York, USA: John Wiley & Sons, 2016
- [22]ANSYS FLUENT Fuel Cell Modules Manual, Ansys Inc, 2011
- [23]Spiegel C. *PEM Fuel Cell Modeling and simulation Using MATLAB*, London, UK: Elsevier/Academic Press, 2008.